CERN-ACC-NOTE-2019-0049

14 November 2019

LHeC optics with $\beta^* = 10$ cm and $L^* = 15$ m

E. Cruz-Alaniz, R. Martin and R. Tomás

Keywords: `LHeC, Interaction Region design, Dynamic Aperture`

Summary

New proton optics have been designed for LHeC taking into account new final focus magnet designs and ensuring a full compatibility with HL-LHC version 1.3. The distance between the interaction point (IP) and the first quadrupole has been increased to 15 m to alleviate synchrotron radiation. The smallest β^* found compatible with magnet aperture is $\beta^* = 10$ cm. Chromaticity correction is demonstrated down to $\beta^* = 7$ cm with acceptable Dynamic Aperture (DA). Ideas and challenges are discussed for $\beta^* = 5$ cm and a new possible final focus based on quadrupole doublets.

Contents

1 Interaction region layout

Since the release of the LHeC conceptual design report in 2012 [1] the linac-ring option with a 50 to 60 GeV Energy Recovery Linac (ERL) has become the baseline design option for the LHeC. This is due to the higher achievable luminosity of the Linac-Ring option, as well as the interference of the installation of an electron ring in the LHC tunnel with its operation [2]. The latest optics designs can be found in [3].

The basic principle of the Linac-Ring IR design remains unchanged and is shown in Figure 1: The two proton beams are brought onto intersecting orbits by strong separation and recombination dipoles. A collision of the proton beams at the IP is avoided via timing. The large crossing angle keeps the long range beam-beam effect small and separates the beams enough to allow septum quadrupoles to focus only the colliding beam (beam 2). The non-colliding beam is unfocused and passes the septum quadrupoles in a field free aperture. The electron beam is brought in with an even larger angle, partly sharing the field free aperture of the septum quadrupoles with the non-colliding beam. A weak dipole in the detector region bends the electron beam into head-on collisions with the colliding proton beam. The two proton beams are also exposed to the dipole field but, due to the large beam rigidity, they are barely affected. After the interaction point a dipole with opposite polarity separates the orbits of the electron and proton beam.

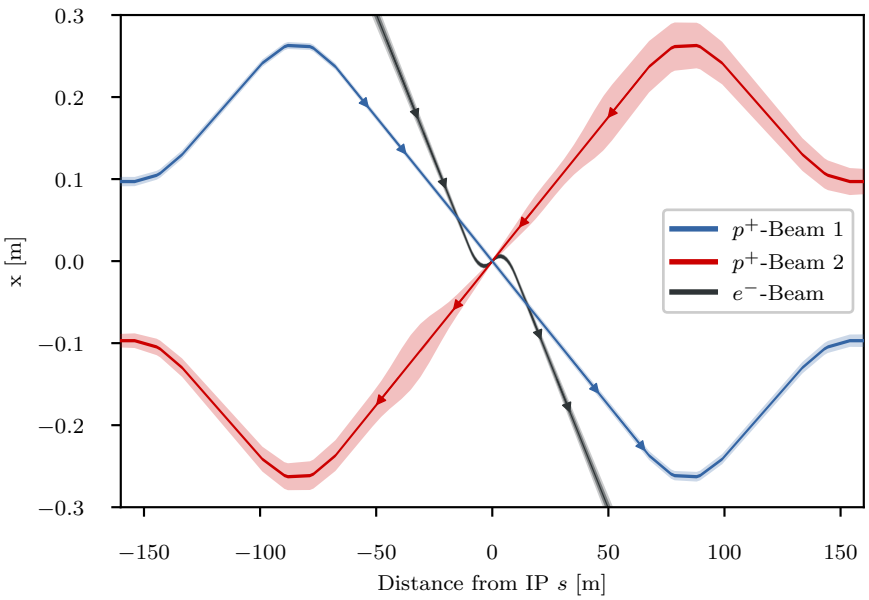

Figure 1: Geometry of the interaction region with 12.3σ envelopes for the proton beams and 5-10σ envelopes for the electron beam.

Some of the parameters of the ERL have changed since the publication of the conceptual design report, e.g. the current, so the parameters are summarized in Table 1. Particularly the increase in current that is necessary for a higher luminosity poses a potential problem for the interaction region (IR) as it increases the already high synchrotron radiation.

The ERL parameters are not the only major change the new IR design has to account for. The first design of the quadrupole septa featured a separation of 68 mm

Table 1: Parameters of the ERL.

Electron beam energy E_e[GeV]	60
Electron beam current I_e[mA]	20 [1]
Normalized emittance $\gamma\epsilon$ [µm]	20
Bunch spacing [ns]	25

[1] Values of 15 mA and 25 mA have also been discussed [4, 5]

Table 2: Parameters of the final focus quadrupole septa. The parameters of Q1a/b and Q2 are compatible with the Nb_3Sn based designs from [7] assuming the inner protective layer of Q2 can be reduced to 5 mm thickness.

Magnet	Gradient [T/m]	Length [m]	Free aperture radius [mm]
Q1a	252	3.5	20
Q1b	164	3.0	32
Q2 type	186	3.7	40
Q3 type	175	3.5	45

for the two proton beams. However, this design focused strongly on providing a field free region for the non-colliding beam. Unfortunately, this lead to a poor field quality for the strongly focused colliding beam. The first quadrupole Q1 was a half quadrupole design effectively acting as a combined function magnet with a dipole component of 4.45 T [6]. The sextupole field component was also prohibitively high. Consequently, a new design approach focusing on the field quality in the quadrupole aperture was necessary. Table 2 summarizes the parameters relevant for the interaction region design. It is noteworthy that the minimum separation of the two beams at the entrance of the first quadrupole Q1a increased from 68 mm to 106 mm requiring a stronger bending of the electron beam. This would increase the already high synchrotron radiation in the detector region even more. In order to compensate this increase, it was decided to increase L^* to 15 m, an approach that was shown to have a strong leverage on the emitted power [5].

The increased separation of the two proton beams, the longer L^* and the overall longer final focus triplet make longer and stronger separation and recombination dipoles necessary. The dipoles differ from the arc dipoles in that the magnetic field in both apertures has the same direction. Consequently the cross talk between both apertures is significant and the maximum reachable field is lower. The new geometry keeps the required field below 5.6 T. The required lengths and strength of these dipoles are listed in Table 3. It should be noted that the inter-beam distance is different for each of the five magnets per side, so each magnet will likely require an individual design. The design of the D1 dipoles is further complicated by the fact that an escape line for neutral collision debris traveling down the beam pipe will be necessary, as well as a small angle electron tagger [1]. These issues have not been addressed so far, further studies will require detailed dipole designs.

The first design of the LHeC interaction region featured detector dipoles occupying almost the entire drift space between the interaction point and first quadrupole. The approach was to have the softest synchrotron radiation possible to minimize the power. However, since the purpose of the dipoles is to create a spacial separation at the entrance of the first quadrupole, it is possible to make use of a short drift

Table 3: Parameters of the separation and recombination dipoles. The respective interbeam distances are given for the magnet with the lowest value.

Magnet	Field strength [T]	Inter-beam distance [mm]	Length [m]	Number
D1	5.6	≥ 496 mm	9.45	6
D2	4.0	≥ 194 mm	9.45	4
IP Dipole	0.21	-	10	2

between dipole and quadrupole to increase the separation without increasing the synchrotron radiation power. A dipole length of $\frac{2}{3}L^*$ is the optimum in terms of synchrotron radiation power [8]. Compared to the full length dipole it reduces the power by 15.6 % at the cost of a 12.5 % higher critical energy. With an L^* of 15 m the optimum length of the detector dipoles is 10 m. A magnetic field of 0.21 T is sufficient to separate the electron and proton beams by 106 mm at the entrance of the first quadrupole. With these dipoles and an electron beam current of 20 mA at 60 GeV the total synchrotron radiation power is 83 kW with a critical energy of 513 keV. If the electron beam energy is reduced to 50 GeV the power is reduced to 40 kW at 297 keV.

A schematic layout of the LHeC interaction region with the dipoles discussed above is shown in Fig. 2. The corresponding beam optics will be discussed in the next section.

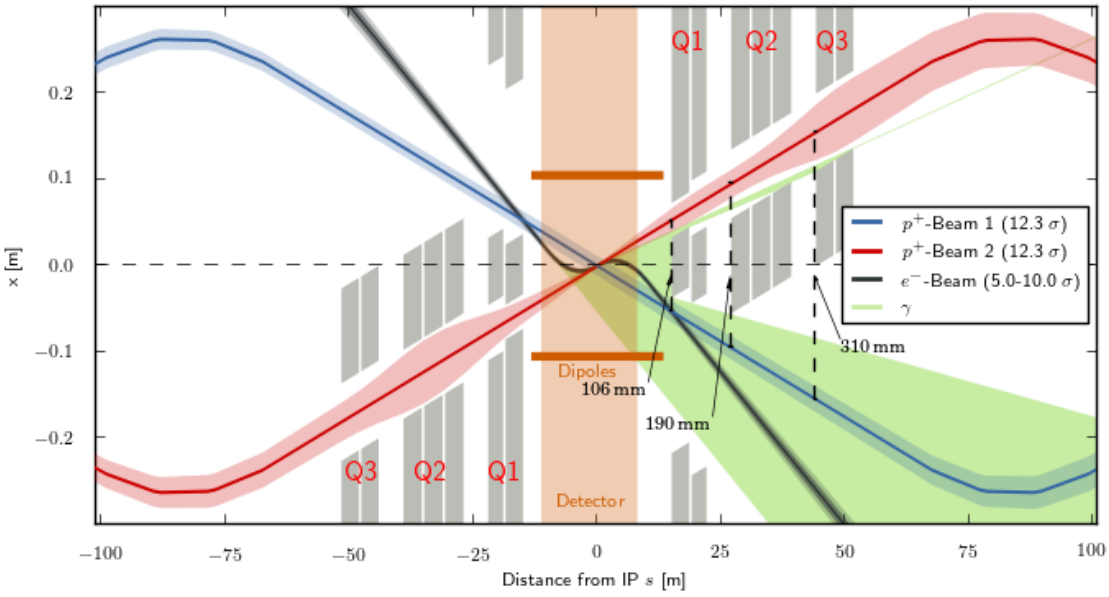

Figure 2: Schematic layout of the LHeC interaction region. The colliding proton beam and the electron beam are shown at collision energy while the non-colliding beam is shown at injection energy when its emittance is the largest.

2 Colliding proton optics

As discussed above, the L^* was increased to 15 m in order to compensate the increased synchrotron radiation due to the larger separation. The final focus system

is a triplet consisting of the quadrupoles Q1a and Q1b (see Table 2), three elements of the Q2 type and two of the Q3 type. Between the elements a drift space of 0.5 m was left to account for the magnet interconnects in a single cryostat. Between Q1 and Q2 as well as Q2 and Q3 a longer drift of 5 m is left for cold-warm transitions, BPMs and vacuum equipment. Behind Q3 but before the first element of the recombination dipole D1 another 16 m of drift space are left to allow for the installation of non-linear correctors in case the need arises, as well as a local protection of the triplet magnets from asynchronous beam dumps caused by failures of the extraction kickers (see Sec. 2.1.1).

As the recombination dipoles D1 and D2 for the LHeC interaction region require more space than the current ALICE interaction region, The quadrupoles Q4 and Q5 had to be moved further away from the IP. The position of Q6 is mostly unchanged but due to a need for more focusing the length was increased by replacing it with two elements of the MQM magnet class of LHC.

With the triplet quadrupole parameters provided in Table 2 we were able to match optics with a minimum β^* of 10 cm. The corresponding optics are shown in Fig. 3 and feature maximum β functions in the triplet in the order of 20 km. With these large β functions, the free apertures of the quadrupoles leave just enough space for a beam stay clear of $12.3\,\sigma$, the specification of the LHC. This is illustrated in Fig 3. However, since the LHeC is supposed to be incorporated in the HL-LHC lattice, this minimum beam stay clear requires specific phase advances from the extraction kicker to the protected aperture. Details will be discussed in Section 2.1. The large β functions not only drive the aperture need in the final focus system, but also the required chromaticity correction in the adjacent arcs. To increase the leverage of the arc sextupoles, the Achromatic Telescopic Squeezing scheme (ATS) developed for HL-LHC [9] was extended to the arc upstream of IP2 (see Fig. 4). This limited the optical flexibility in the matching sections of IR2, specifically of the phase advances between arc and IP2. As a consequence, the optical solution we found (Fig. 3) still has a residual dispersion of 15 cm at the IP and the polarities of the quadrupoles Q4 and Q5 on the left side of the IP break up the usual sequence of focusing and defocusing magnets. It needs to be studied whether this is compatible with possible injection optics. The free apertures given in Table 2 include a 10 mm thick shielding layer in Q1 and 5 mm in Q2 and Q3. This is necessary to protect the superconducting coils from synchrotron radiation entering the magnets as can be seen in Figure 2. The absorber must also protect the magnets from collision debris. Simulations of both synchrotron radiation and collision debris are yet to be conducted in order to confirm the feasibility of this design.

A separation between the two proton beams in time is currently foreseen, i.e. while the orbits of the two proton beams do cross, the bunches do not pass through the IP at the same time. This approach is complicated by the fact that the timing of the bunches in the other three interaction points should not be affected. The easiest way to accomplish this is by shifting the interaction point of LHeC by a quarter of a bunch separation, i.e. $6.25\,\text{ns} \times c \approx 1.87\,\text{m}$ upstream or downstream of the current ALICE IP. This will of course have an impact in the integration of the detector in the underground cavern [10], however it seems feasible [11].

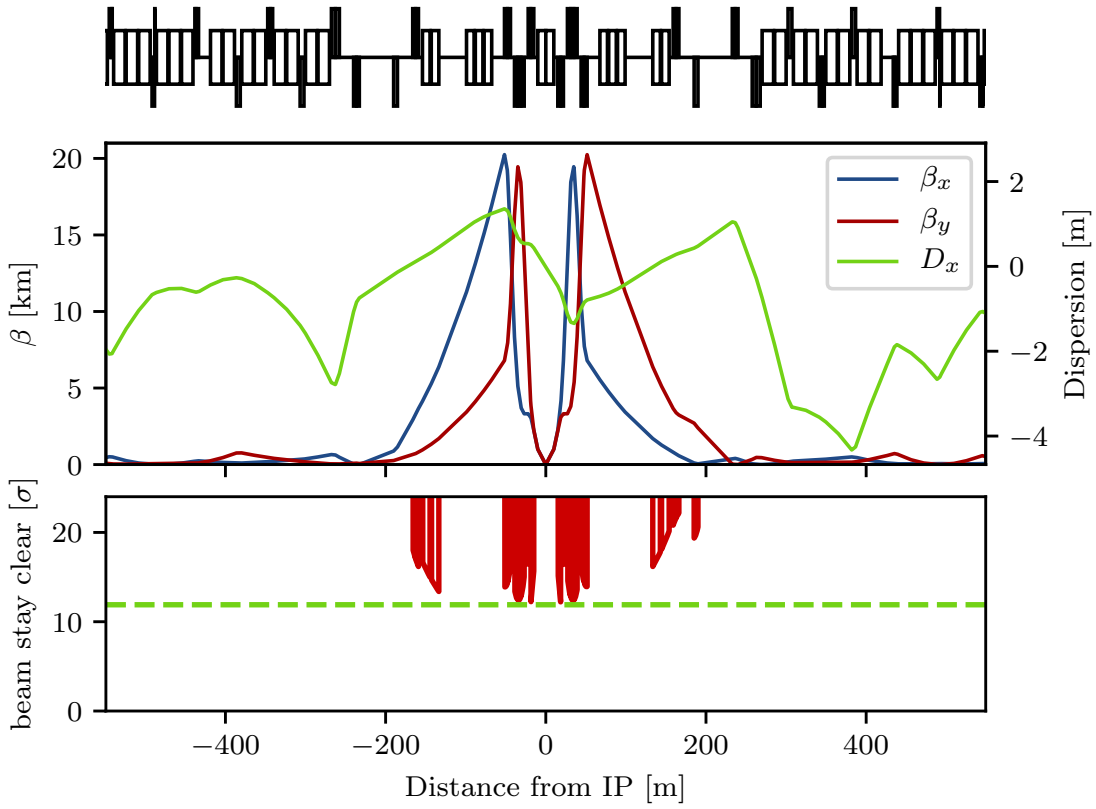

Figure 3: Optics (top) and beam stay clear (bottom) of the colliding beam with $\beta^* = 10\,\text{cm}$.

2.1 Arc integration

This section explains the integration of the interaction region explained in the previous section into the HLLHCV1.3 version of the HL-LHC lattice. This integration had been done for a previous version (HLLHCV1.0), but the need of an integration to a more updated design, as well as new aperture requirements (described also in this section) motivated the need for a new integration. The description of the chromaticity correction, status of cases with low β^* and dynamic aperture are also addressed here.

2.1.1 Aperture requirements

The LHeC experiment is supposed to replace the ALICE detector in the HL-LHC, the other experiments will remain in the ring and take data. This means LHeC must not compromise the other interaction points but it also means it must adhere to the same aperture constraints as the rest of the HL-LHC. For the initial design a minimum beam stay clear of $12.3\,\sigma$ was adapted from the LHC specification. However, newer studies for the HL-LHC show that the protected aperture significantly depends on the phase advance between the extraction kicker and the local aperture protection [12]. This is due to the oscillation trajectory of bunches deflected during the kicker rise time in the event of an asynchronous beam dump. With a phase advance of 0° or 180° from the kicker to the protected aperture, a direct hit should

be unlikely, so aperture bottlenecks should be close to that. For a beam stay clear of $12.3\,\sigma$ a phase advance of less than 30° from either 0° or 180° was calculated to be acceptable [12]. The major complication comes from the fact that not only the final focus system of LHeC, but also of the two main experiments ATLAS and CMS need to have to correct phase advances and since the phase advances between IP2 (LHeC) and IP1 (ATLAS) are locked in the achromatic telescopic squeezing scheme there are few degrees of freedom to make adaptations.

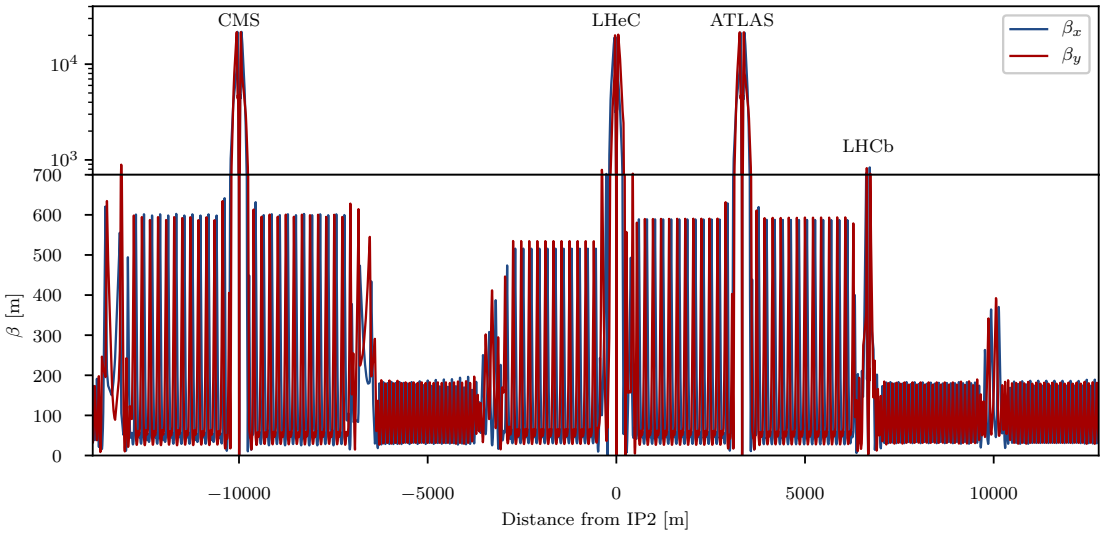

Figure 4: Optics of full ring of the colliding beam 2.

2.1.2 Achromatic Telescopic Squeezing

The Achromatic Telescopic Squeezing (ATS) scheme [9] is a novel optical solution proposed for the HL-LHC to strongly reduce the β^* while controlling the chromatic aberrations induced, among other benefits.

The principles of the ATS as implemented for the HL-LHC are as follows: first, in the preesqueeze stage, a standard matching procedure is performed in the interaction regions to obtain a value of β^* which is achievable in terms of quadrupole strengths and chromaticity correction efficiency, in the case of HL-LHC this corresponds to IR1 and IR5. A further constraint at this point is to match the arc cell phase advance on the regions adjacent to the low β^* interaction regions to exactly $\pi/2$. Later, at the collision stage, the low β^* insertions remain unchanged and instead the adjacent interaction regions contribute to the reduction of β^*, that is IR8 and IR2 for IR1, and IR4 and IR6 for IR5. The $\pi/2$ phase advance allows the propagation of β-waves in the arc. If phased correctly with the IP, these β-waves will reach their maximum at every other sextupoles, increasing the β function at their location at the same rate that the decrease in β^*. The increase of the β function at the location of the sextupoles will result in an increase of their efficiency, allowing the system to correct the high chromaticity produced by the high-β function in the inner triplet. This way, the ATS allows a further reduction of the β^* at the same time that correcting the chromaticity aberrations produced in the low β insertions.

Following the experience for HL-LHC, the ATS scheme was proposed for the

LHeC project to overcome some of the challenges of this design in terms of limits in the quadrupole strengths of the interaction region and in the chromaticity correction.

A first integration of the LHeC IR into the HL-LHC lattice using the ATS scheme for the previous nominal case with $\beta^* = 10\,\text{cm}$ and $L^* = 10\,\text{m}$ was presented by extending the β wave into the arc 23 [5]. The flexibility of this design was later explored to study the feasibility of minimizing β^*, to increase the luminosity, and increasing L^*, to minimize the synchrotron radiation. It was found that increasing L^* to 15 m provided a good compromise but keeping the β^* to 10 cm.

2.1.3 New Lattice

Using the consideration explained in the previous sections, the following changes have been made to the HLLHCV1.3 lattice [13] to obtain the LHeC lattice. Starting with the presqueeze optics ($\beta^* = 55\,\text{cm}$ in IR1 and IR5), the arc cell phase advance in arc 23 is changed to $\pi/2$. The global phase change can be recovered using the arc phase in arcs 34, 67 and 78. At this stage, it is also convenient to use these arc phases such that the phase advance from the kicker to IP1 and IP5 is less than 30 degrees, as specified in Section 2.1.1. The old IR2 is now removed and the new matched IR is installed in the lattice and matched to obtain the presqueeze optics in IR2 ($\beta^* = 30\,\text{cm}$), while keeping the same values at the ends of IR2. A further consideration at this stage is having the horizontal and vertical phase advance left and right to the IR to 2.95 and 2.7 (in units of 2π), respectively.

Once the presqueeze optics was achieved an iterative process was done to obtain the collision optics for all three IRs (IR1, IR2, and IR5), which is described in the following:

1. Rematch of all IRs and arcs to the corresponding values, but given the complexity of each IR matching, the collision optics already found for the HL-LHC regions (around IR5 and IR1) and for LHeC (described in Section 2) was used as initial guess.

2. Match the values of the corresponding correctors to give the appropriate crossing angle at all interaction points (IP1, IP2, IP5 and IP8) and correct the spurious dispersion arising from such crossings.

3. Correct tune and chromaticity as described in Section 2.1.4, and Section 2.1.5 for the case with lower β^*.

4. Make sure the resulting lattice still fulfills the appropriate phasing conditions (less than 30 degrees from kicker in IR6 to IP1, IP2 and IP5). If it has shifted with the matching use the arc cell phase of the non-ATS arcs (34, 67 or 78) to adjust and repeat the process again.

At the end of this iterative process we obtain a lattice for the required collision optics in all IRs (β^*=15 cm for IR1 and IR5 and β^*=10 cm for IR2), with the appropriate corrections (crossing, dispersion, tune and chromaticity). The phases between the extraction kicker in IR6 and the different low β^* triplets were also checked, resulting in 15° from the horizontal for IR1, 22° for IR2 and 26° for IR5, therefore fulfilling the <30°requirement for all three IRs.

2.1.4 Chromaticity Correction

The chromaticity correction for the LHeC lattice further develops from the HL-LHC chromaticity correction scheme. The strong families (SF2 and SD2 in arcs 12, 23, 45, 56, 78 and 81) as well as the weak defocusing families (SD1 in arcs 12, 23, 45, 56 and 78) are allowed to vary independently while the focusing weak families (SF1 in arcs 12, 23, 45, 56, 78 and 81) are set to a value of 0.06 (to keep the same values as the HL-LHC lattice), and not changed. The non-ATS sextupole families (SF1, SF2, SD1 and SD2 in arcs 34, 67 and 78) are set to have the same strengths and allowed to vary by the same amount. The limit on the sextupoles were set to 4430 $\mathrm{T/m^2}$ (corresponding to I_{max}=550 A) which was enough to correct the chromaticity for the case with $\beta^* = 10\,\mathrm{cm}$ but it becomes more challenging for cases with lower β^*, this was later fixed by using a different method, as explained in section 2.1.5.

A different method varying all sextupole families independently was also tested and was able to correct the chromaticity for the case with β^*=10 cm, just as it was done for the previous case with L^*=10 m [5]; however, the first method converged must faster and therefore was selected as the preferred option.

2.1.5 Chromaticity correction with β^* below 10 cm

Previously, cases with lower β^* were obtained by using the baseline case with β^* of 10 cm and varying the quadrupoles of the same interaction region (IR2) to obtain the desired β^* at the interaction point. Following this method, cases with β^*=5,7,8 and 9 cm and L^*=10 cm were found [5] but with some considerable drawbacks: first, the gradient limits and aperture constraints of the quadrupoles used for the matching were not strictly kept, and secondly, the chromaticity correction increased, this time without increasing β functions at sextupoles, and therefore the chromaticity correction was no longer achievable for the case with $\beta^* = 5\,\mathrm{cm}$; furthermore, this limit is expected to worsen when increasing L^* to the new baseline of 15 m.

In order to address such drawbacks, a new method was implemented that consisted in using the same principle of ATS and allow the adjacent IR3 to contribute to the lower β^* in IR2, this time the β function increases in the arc 23 and consequently also its correction efficiency. The quadrupoles in IR2 are used to keep the optical functions at the other side of IR2 (towards IR1) same as before, to keep the HL insertions and arc 12 untouched. With this method, lattices with β^*= 7, 8 and 9 cm and $L^* = 15$ m were successfully matched in terms of both the β^* and the chromaticity correction. It must be noted however that these cases require a larger aperture in the inner triplet.

2.2 Dynamic Aperture

Dynamic aperture studies were performed to analyze the stability of the lattice designs.

DA studies were performed using SixTrack [14] on a thin-lens version of the LHeC lattice at collision ($\beta^* = 0.15\,\mathrm{m}$ in IP1 and IP5, $\beta^* = 10\,\mathrm{cm}$ in IP2) over 10^5 turns with crossing angles on, 30 particles pairs per amplitude step of $2\,\sigma$, 5 angles in the transverse plane and a momentum offset of 2.7×10^{-4}. The energy was set to 7 TeV and the normalised emittance to $\epsilon = 2.5\,\mu\mathrm{m}$. No beam-beam effects were included in this study.

Previous DA studies had been performed for a previous version of the LHeC lattice [5]. These studies did not include triplet errors of either of the low-β interaction regions, as these errors were not available at that stage. These studies were updated for the newer version of the LHeC lattice described in the previous sections and included errors on the triplets of IR1 and IR5. For the case of IR2 errors tables for the new triplet are not yet available but it was estimated that the same field quality than the triplets for the HL IR can be achieved for these magnets, and therefore the same field errors were applied but adjusted to the LHeC triplet apertures.

The initial DA resulted in $7\,\sigma$ but following the example of HL-LHC and FCC studies [15] two further corrections were implemented: the use of non-linear correctors to compensate for the non linear errors in the LHeC IR, and the optimization of the phase advance between IP1 and IP5. With these corrections the DA was increased to $10.2\,\sigma$, above the target of $10\,\sigma$. The case for lower β^*, particularly for the case of interest with $\beta^* = 7\,\text{cm}$ proved to be more challenging, as expected, when adding errors on the LHeC IR; however with the use of the latest corrections a DA of $9.6\,\sigma$ was achieved, that is not far off from the target. Fig. 5 shows the DA vs angle for both these cases. It is important to point out that the challenge for the β^*=7 cm case comes instead from the quadrupole aperture and gradient requirements, particularly in the first magnet.

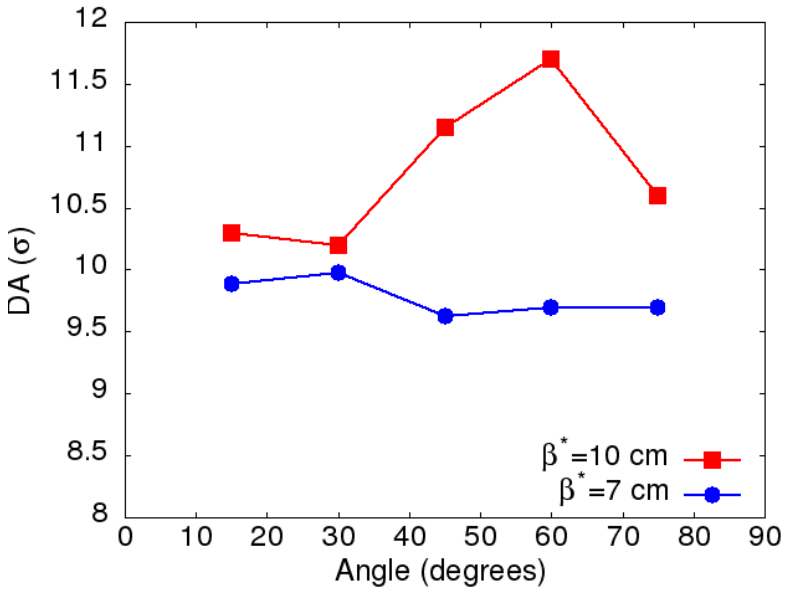

Figure 5: Dynamic aperture vs angle for 60 seeds for the LHeC lattice at collision for the cases $\beta^* = 10$ cm (red) and $\beta^* = 5$ cm in IP2.

2.3 Ideas and challenges for $\beta^* = 5$ cm

The proton optics described in the previous chapters featured a minimum β^* of 10 cm. However, from the particle physics point of view a lower β^* is desirable in order to maximize the luminosity. A value of down to 5 cm is requested from the experiments. This will require a completely different final focus system as the lower β^* means the beam size in the triplet will become larger. Larger apertures are required and consequently the gradients in the quadrupoles will decrease. However

similar integrated focusing strengths will be required so the overall length of the triplet will increase. As this will in turn increase the β functions in the triplet further it is imperative to get the most out of the available space. An example of available space is the drift between the detector region dipoles and the triplet magnets as shown in Fig. 6. The optimum dipole lengths in terms of synchrotron radiation power was determined to be $2/3 \cdot L^*$ so a drift of 5 m is left. Now it is immediately clear that this region cannot be occupied by a superconducting septum quadrupole as that would effectively decrease L^* and thus increase the synchrotron radiation power as a stronger separation is necessary. Instead it is thinkable that a normal conducting quadrupole septum can be built that either does not require a yoke or similar structure between the beams or has a very thin yoke, or a septum that has a very limited and controlled field in the region of the electron beam trajectory. In the later case it might even be used as part of the final focus system of the electron beam. Either way, it is clear that such a normal conducting septum must have a pole tip field way below the saturation limit of iron. For our calculation a pole tip field of 1 T was assumed. For $\beta^* = 5$ cm an aperture radius of 20 mm is required at a distance of 14 m from the IP, resulting in a pole tip field of 50 T/m for the normal conducting septum called Q0. Possible ratios of apertures and gradients for the remaining triplet magnets were approximately based on the quadrupole parameters shown in Table 2, however these parameters would require a magnet design for confirmation. With the quadrupole parameters shown in Table 4 we were able to obtain triplet optics that can accommodate a beam with a minimum β^* of 5 cm.

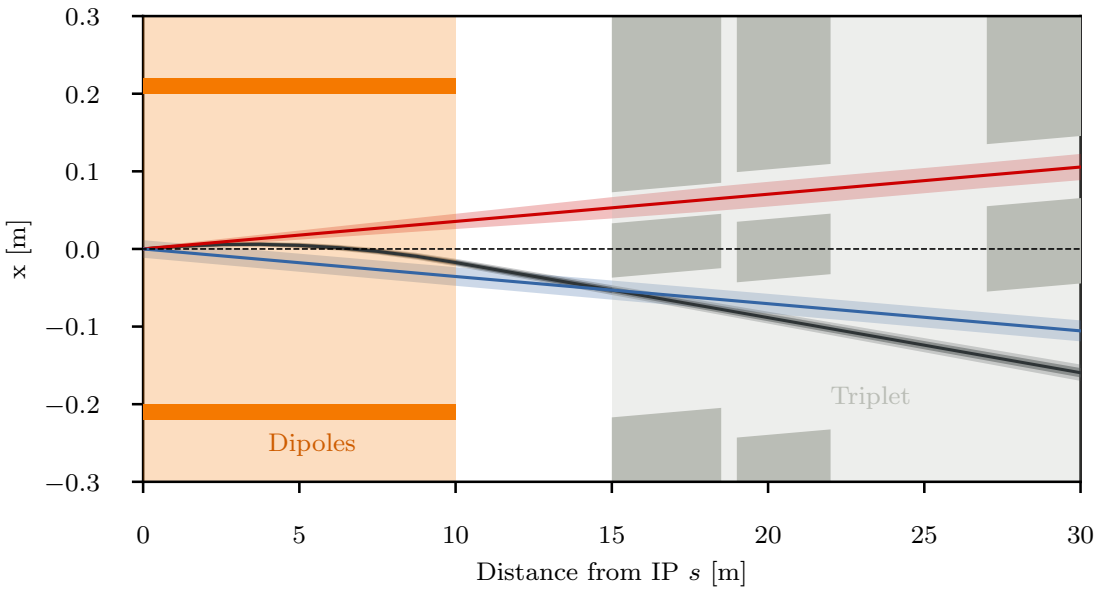

Figure 6: Empty space between the detector dipole and the superconducting quadrupoles of the final focus triplet.

The corresponding optics are shown in Fig. 7. So from the triplet point of view it appears possible to reach the requested minimum β^*, however there are many assumptions that need verification: First the magnetic design for the normal conducting quadrupole septum must be shown to be possible. If there is a residual field in the space of the electron beam trajectory, the impact on the electron beam and the synchrotron radiation power must be evaluated. The parameters of the

Table 4: Parameters of the final focus quadrupole septa required to accommodate a β^* of 5 cm. The normal conducting quadrupole is called Q0 although it has the same polarity as Q1a/b.

Magnet	Gradient [T/m]	Length [m]	Aperture radius [mm]
Q0 (nc)	50	3.0	20
Q1a	110	3.5	27
Q1b	162	5.0	37
Q2	123	5.0	62
Q3	123	4.5	62

modified superconducting triplet quadrupole septa, although scaled conservatively, must be confirmed. Furthermore the larger aperture radius of Q1 might require a larger separation at the entrance of Q1, increasing the synchrotron power that is already critical. Thus a full design of such magnets is required. Lastly, the interaction region must be integrated into the full ring to verify that chromaticity correction is possible. The studies in Section 2.1.5 that were conducted on the normal triplet without regard for aperture constraints suggest that a chromaticity correction is only possible for a β^* down to around 7 cm.

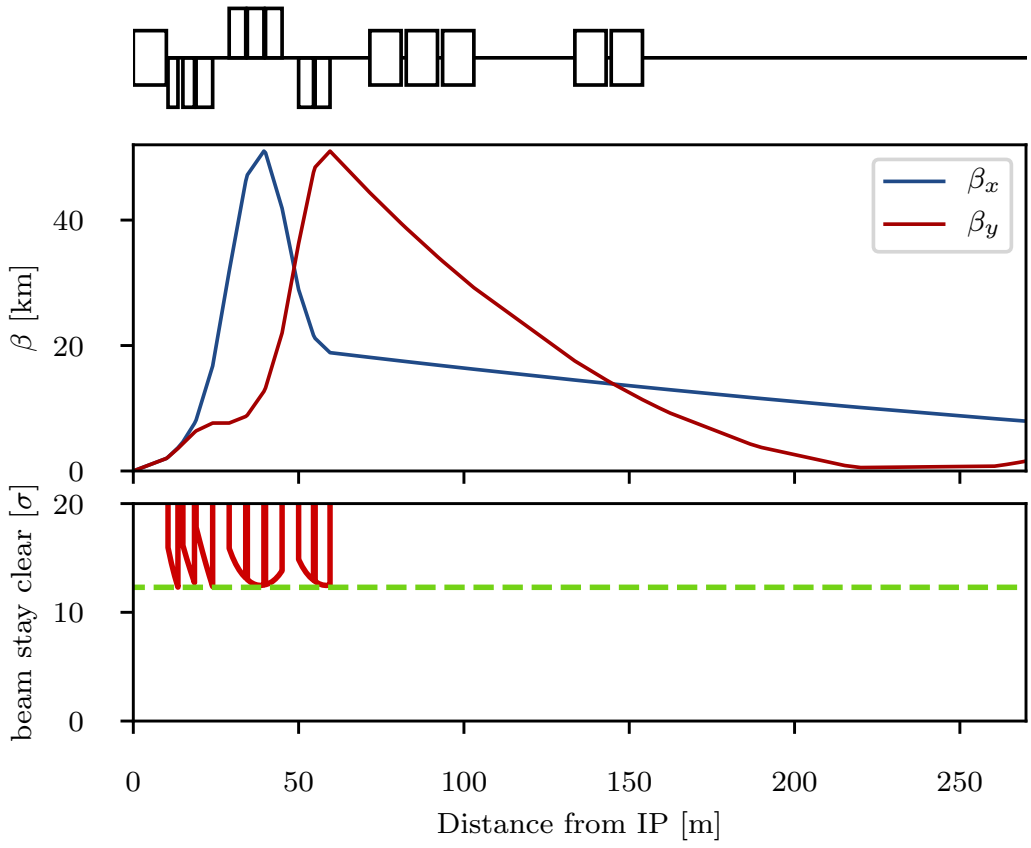

Figure 7: Optics (top) and beam stay clear (bottom) in the triplet region of colliding beam with $\beta^* = 5$ cm.

2.4 Alternative approach to the final focus system using a doublet

So far the approach to the optics of the final focus system was a triplet. The triplets on either side of the IP are antisymmetric. This is inherited from the ALICE final focus system where the aperture is shared and the antisymmetry guarantees the same optics for both beams and similar chromaticities in both horizontal and vertical planes. In the LHeC final focus system however, the apertures of the quadrupoles are not shared between both beams, so the antisymmetry is not strictly necessary, although it eases the integration in the full ring. An alternative approach that is worth studying is a symmetric doublet. Doublets feature a large β function in one plane and a relatively low one in the other plane. Since the non-colliding proton beam is of no concern for LHeC it makes sense to create doublets on either side of the IP that have the peak β function in the horizontal plane as the limiting sextupoles in the studies above were the vertically correcting ones. Furthermore, in a doublet the integrated focusing strength needed is lower as fewer quadrupoles act against each other. This further reduces the chromaticity and should also reduce the overall length of the final focus system. With the space saved by the doublet it is possible to either shift the recombination dipoles D1 and D2 closer to the IP, reducing the needed integrated strengths, or even to increase L^* to further reduce the synchrotron radiation power and critical energy. In order to make best use of the available doublet quadrupole aperture, it is also thinkable to collide with flat beams. The main disadvantage of symmetric doublets is the breaking of the sequence of focusing and defocusing quadrupoles. As no changes should be made to the arcs, the left-right symmetry needs to be broken up again in one of the matching sections, either by introducing another quadrupole on one side of the IP, or by overfocusing the beam.

3 Non-colliding proton beam

At collision energy the non-colliding beam has no optics specification within the straight section. Consequently we only need optics to transfer the beam from the left arc to the right arc without hitting the aperture and at a specific phase advance. The same is true at injection energy, just with a larger emittance, making satisfaction of the aperture constraint more difficult. Thus it is sufficient to find working injection optics, as no squeeze will be required for this beam. This approach of course will require some tweaks as at least one arc will apply the ATS scheme at collision, but as the aperture constraint is less tight at higher energy there should be enough degrees of freedom available.

Finding injection optics appears trivial at first but is complicated by the fact that the distance between the IP and the first quadrupole magnet Q4 is larger than 159 m. A total distance of 318 m needs to be bridged without any focusing available. To add to this the matching quadrupoles Q4 and Q5 act as a focusing doublet where the peak β functions (and thus the aperture bottlenecks) are to be expected in Q5. Thus we concluded that optics with $\beta^* = L^*$ (with β^* the β function at the IP and L^* the distance between IP and the first quadrupole, Q4) and $\alpha^* = 0$ will give a minimum β^* at Q4 but are not the optimum for Q5. Instead the β^* was slightly reduced and an $\alpha^* \neq 0$ was introduced. While this approach increases the peak β in

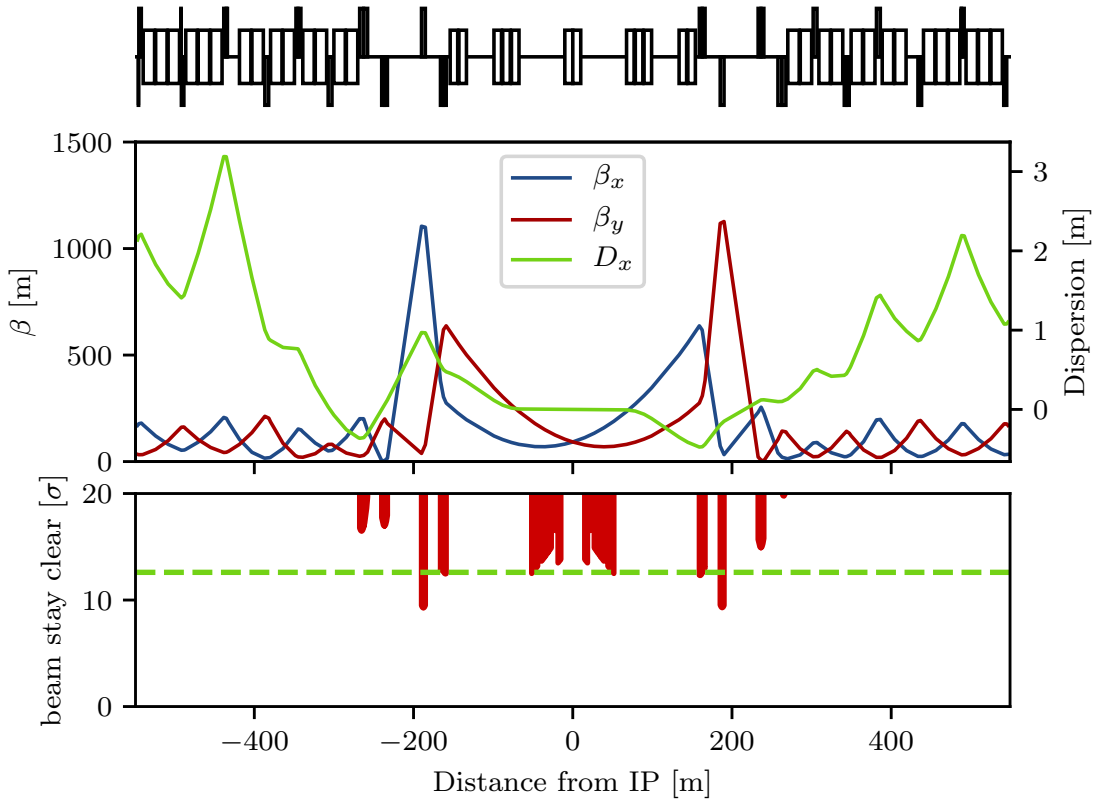

Figure 8: Optics (top) and beam stay clear of the non-colliding beam at injection energy. The Q5 quadrupole magnets on either side of the IP currently are aperture bottlenecks. It should be possible to mitigate this problem by replacing the magnets with longer, larger aperture magnets.

Q4 the peak in Q5, where the bottleneck is expected, is reduced. At the same time the beam size at the beginning of the septum quadrupole must not exceed about 32 mm in diameter in order to fit through the field free region at the given angle of 7.2 mrad between the two proton beams. We found that optics with $\beta^* = 92$ m and $\alpha^* = \pm 0.57$ are close to the optimum beam size in the quadrupole septa and Q4. The corresponding optics are shown in Fig. 8. For the magnets Q4 and Q5 LHC quadrupoles of the large aperture MQY type with 70 mm aperture diameter and a 160 T/m gradient were assumed. As can be seen in the aperture plot, the triplet quadrupole septa and Q4 are just below the minimum beam stay clear at injection of $12.6\,\sigma$. With some minor tweaks in the optics these should not be an issue. However the Q5 magnets only have a beam stay clear of about $9.2\,\sigma$ with little chance of decreasing the beam size without increasing it both in Q4 and in the quadrupole septa. Consequently it will be necessary to use quadrupoles with even larger apertures (at least 106 mm with current optics) and make up for the lower gradient by increasing the length or by using Nb_3Sn technology. At injection energy the remaining magnets in the IR have strengths according to the HL-LHC specification and thus do not pose any problems. However the injection optics shown in Fig. 8 will require some changes during the ramp as Q4, Q5 and Q6 would become too strong at collision energy. This is not considered a problem though, as the emittance shrinking will ease the aperture requirements.

The non-colliding proton beam does not need to be focused and consequently passes the quadrupole septa of the colliding beam in the field free region. The large angle of 7200 µrad between the two beams (compared to 590 µrad in the high luminosity IPs) should suffice to mitigate long range beam-beam effects, considering that the shared aperture is only 30 m long as opposed to the main experiments where the shared aperture exceeds a lengths of 70 m.

4 Electron beam

Many questions are still open concerning the design of the electron interaction region of LHeC. In the past, basic interaction region designs with and without chromaticity correction were presented [16, 17] but were never integrated in the whole ERL. To allow integration with proton beam line, the electron final quadrupoles were placed at 30 m from the IP [18], which should still be compatible with the new proton L*=15 m, see Fig. 2. Without chromaticity correction in the electron final focus, aberrations at the IP decrease luminosity by about 20% [19]. Lattices including chromaticity correction had a significant length of 150 m. However, the whole straight section between Linac and ERL arc is only 290 m long [1] and the IR design did not include a matching and splitting section or a focus system for the spent, outgoing electron beam.

Alternatively, it is possible to think of an electron final focus system between the detector dipoles and the first quadrupole septum of the colliding proton beam. In that case the L^* of the electron beam would be around 11 m, which significantly eases chromaticity correction. Again, the proton beams should not be affected significantly, but must be accommodated in the design of the normal conducting quadrupoles.

Lastly, the current electron beam shown in Fig. 2 has a β^* chosen to simply match the beam size of the colliding proton beam at $\beta^* = 10$ cm. No higher order effects like pinching have been studied for this parameter.

References

[1] J. L. Abelleira Fernandez et al. A large hadron electron collider at CERN report on the physics and design concepts for machine and detector. *Journal of Physics G: Nuclear and Particle Physics*, 39(7):075001, Jul 2012.

[2] Oliver Brüning. Accelerator design. Presented at the LHeC Workshop, June 2015.

[3] Lattice repository. https://gitlab.cern.ch/lhec-optics/lhec-lattice, 2019.

[4] Oliver Brüning, John Jowett, Max Klein, Dario Pellegrini, Daniel Schulte, and Frank Zimmermann. Future Circular Collider Study FCC-he Baseline Parameters. Technical Report EDMS 17979910, FCC-ACC-RPT-0012, CERN, Geneva, Apr 2017.

[5] E. Cruz-Alaniz, D. Newton, R. Tomás, and M. Korostelev. Design of the large hadron electron collider interaction region. *Phys. Rev. ST Accel. Beams*, 18:111001, Nov 2015.

[6] Brett Parker. Latest Developments and Progress on the IR magnet design. presented at the LHeC and FCC-eh Workshop, Sept 2017.

[7] Brett Parker. Superconducting Magnet Concepts for Electron Hadron Collider IRs. presented at the Electrons for the LHC - LHeC/FCCeh and Perle Workshop, Sept 2018.

[8] Roman Martin and Rogelio Tomás Garcia. Length optimization of the detector region dipoles in LHeC and FCC-eh. Technical Report CERN-ACC-2018-0042, CERN, Geneva, Oct 2018.

[9] Stéphane Fartoukh. Achromatic telescopic squeezing scheme and application to the lhc and its luminosity upgrade. *Phys. Rev. ST Accel. Beams*, 16:111002, Nov 2013.

[10] Andrea Gaddi. Installation Issues of eh Detectors (LHC and FCC). presented at the LHeC and FCC-eh Workshop, Sept 2017.

[11] Andrea Gaddi. Private communication, Jan 2019.

[12] Roderik Bruce, Chiara Bracco, Riccardo De Maria, Massimo Giovannozzi, Stefano Redaelli, Rogelio Tomás Garcia, Francesco Maria Velotti, and Jörg Wenninger. Updated parameters for HL-LHC aperture calculations for proton beams. Technical Report CERN-ACC-2017-0051, CERN, Geneva, Jul 2017.

[13] Lattice repository:/afs/cern.ch/eng/lhc/optics/HLLHCV1.3.

[14] Sixtrack web site: http://sixtrack.web.cern.ch/SixTrack/.

[15] van Riesen-Haupt L. Seryi A. R. Martin Cruz-Alaniz E., Abelleira J.L. and Tomás R. Methods to increase the dynamic aperture of the fcc-hh lattice. In *Proc. of International Particle Accelerator Conference (IPAC'18), Vancouver,*

Canada, 2018, number 1 in International Particle Accelerator Conference, pages 3593–3596, Geneva, Switzerland, May 2018. JACoW.

[16] Frank Zimmermann et al. Interaction-Region Design Options for a Linac-Ring LHeC. In *Proc. of International Particle Accelerator Conference (IPAC'10), Kyoto, Japan, May 23-28, 2010*, number 1 in International Particle Accelerator Conference, pages 1605–1607, Geneva, Switzerland, May 2010. JACoW.

[17] J. L. Abelleira, H. Garcia, R. Tomás, and F. Zimmermann. Final-Focus Optics for the LHeC Electron Beam Line. In *Proc. of International Particle Accelerator Conference (IPAC'12), New Orleans, Louisiana, USA, May 20-25, 2012*, number 1 in International Particle Accelerator Conference, pages 1861–1863, Geneva, Switzerland, May 2012. JACoW.

[18] G. Arduini *et al.* Energy frontier dis at cern: the lhec and the fcceh, perle. https://pos.sissa.it/316/183/pdf.

[19] Rogelio Tomás. Lhec interaction region. presented at DIS 2012 Workshop, https://indico.cern.ch/event/153252/contributions/1396962/attachments/160393/226540/SLIDES.pdf, 2012.